

Chapter 2

Effects of Single Metal-Ion Doping on the Visible-Light Photo-reactivity of TiO₂

The text of this chapter has been accepted for publication in *Journal of Physical Chemistry C*
Choi, J.; Park, H.; Hoffmann, M.R. November 2009.

Abstract

Titanium dioxide (M-TiO₂), which was doped with 13 different metal ions (i.e., silver (Ag⁺), rubidium (Rb⁺), nickel (Ni²⁺), cobalt (Co²⁺), copper (Cu²⁺), vanadium (V³⁺), ruthenium (Ru³⁺), iron (Fe³⁺), osmium (Os³⁺), yttrium (Y³⁺), lanthanum (La³⁺), platinum (Pt⁴⁺, Pt²⁺), and chromium (Cr³⁺, Cr⁶⁺)) at doping levels ranging from 0.1 to 1.0 atom-% was synthesized by standard sol-gel methods and characterized by X-ray diffraction (XRD), BET surface area measurement, SEM, and UV-Vis diffuse reflectance spectroscopy (DRS). Doping with Pt(IV), Cr(III), V(III), and Fe(III) resulted in a lower anatase to rutile phase transformation (A-R phase transformation) temperature for the resultant TiO₂ particles, while doping with Ru(III) inhibited the A-R phase transformation. Metal-ion doping also resulted in a red-shift of the photophysical response of TiO₂ that was reflected in an extended absorption in the visible between 400 and 700 nm. In contrast, doping with Ag(I), Rb(I), Y(III), and La(III) did not result in a red-shift of the absorption spectrum of TiO₂. As confirmed by elemental composition analysis by Energy Dispersive X-ray Spectroscopy (EDS), the latter group of ions was unable to be substituted for Ti(IV) in the crystalline matrix due to their incompatible ionic radii. The photocatalytic activities of doped TiO₂ samples were quantified in terms of the photo-bleaching of methylene blue (MB), the oxidation of iodide (I⁻), and the oxidative degradation of phenol in aqueous solution both under visible-light irradiation ($\lambda > 400$ nm) and under broader-band UV-vis irradiation ($\lambda > 320$ nm). Pt- and Cr-doped TiO₂, which had relatively percentages of high rutile in the particle phase, showed significantly enhanced visible-light photocatalytic activity for all three reaction classes.

Introduction

Titania (TiO_2) has been extensively studied as a photocatalyst for applications such as water and air remediation because of its relatively high photocatalytic activity, robust chemical stability, relatively low production costs, and non-toxicity. Redox reactions of environmental interests are initiated on the TiO_2 surface with trapped electron-hole after band-gap excitation. However, TiO_2 is active only under near-ultraviolet irradiation due to its wide band gap energy of $3.0 \sim 3.2$ eV. Therefore, significant efforts have been made over the last 20 years to develop modified TiO_2 particles that are active under visible-light irradiation ($\lambda > 400$ nm). Various strategies have been pursued including doping with metal ions (e.g., iron,¹⁻³ nickel,^{4,5} vanadium,⁶⁻⁸ and chromium⁹⁻¹¹) or nonmetallic element (e.g., nitrogen,¹²⁻¹⁴ sulfur,^{15,16} and carbon^{17,18}).

Metal ion-doped TiO_2 has been primarily studied to enhance the photocatalytic activity under UV irradiation.¹⁹⁻²³ Choi et al.¹⁹ reported that doping with Fe^{3+} , Ru^{3+} , V^{4+} , Mo^{5+} , Os^{3+} , Re^{5+} , and Rh^{3+} ions increased photoactivity for the degradation of CHCl_3 under UV irradiation, whereas doping with Co^{3+} and Al^{3+} decreased photoactivity. The relative photocatalytic efficiency of a metal-ion dopant depends on whether it serves as a mediator of interfacial charge transfer or as a recombination center. Chen et al.²² also showed that Fe- or Ni-doped TiO_2 have higher photoactivities than undoped TiO_2 under UV irradiation.

Numerous metal ions have been investigated as potential dopants including iron,¹⁻³ nickel,^{4,5} vanadium,⁶⁻⁸ chromium,⁹⁻¹¹ platinum,²⁴ ruthenium,²⁵ and cobalt ions.^{26,27} However, there are conflicting results on the effects of doping on the visible-light photoactivity of TiO_2 . The wide-variability in reported impact on visible light activity

may be due to the specific preparation methods, the actual photolysis and experimental conditions used to quantify activity, and broad array of chemical reactions used to verify photoactivity over a broad range of wavelengths at $\lambda > 400$ nm. For example, metal ion-doped TiO₂ is prepared in the form of powders^{2,25,27} and films^{6,7} by different synthetic methods such as sol-gel syntheses,^{6,8,11} MOCVD,¹ hydrothermal synthesis,³ solid-state reactions,⁴ and ion implantation.^{10,28} Photoactivity in the visible has been quantified using a wide array of substrates including dyes,^{1,3,6,8,11} phenolic compounds,^{2,24,29} acetaldehyde,^{6,27} and nitric oxide.^{10,28} Therefore, it is difficult to compare the net effects of metal-ion dopants on the photocatalytic activity of TiO₂. Several reports³⁰⁻³² compare the effects of metal-ion dopants on visible-light photocatalytic activities of TiO₂ using high-throughput (HT) screening techniques. However, the physicochemical properties of various doped TiO₂ samples were not made in such combinatorial approaches.

Herein, we report on the synthesis of sol-gel TiO₂ doped with 13 different metal ions and compare the effects of individual dopants on the resulting physicochemical properties (e.g., a crystal structure and UV-vis absorption) and their corresponding photocatalytic activities with respect to the catalysis of several reactions under visible-light irradiation ($\lambda > 400$ nm). In this regard, the photocatalytic activities of metal ion-doped TiO₂ are quantified in terms of the photo-bleaching of methylene blue (MB), the oxidation of iodide (I⁻), and the degradation of phenol in aqueous suspensions.

Experimental

Chemicals

The specific reagents used in this study include: titanium tetraisopropoxide (TTIP, Aldrich), absolute ethanol (Mallinckrodt), nitric acid (HNO_3 , Aldrich), methylene blue (MB, J.T. Baker), potassium iodide (KI, EM Science), and phenol (Mallinckrodt). The metal ion salts used in the preparations include: AgNO_3 (Mallinckrodt), $\text{Cu}(\text{NO}_3)_2 \cdot 4\text{H}_2\text{O}$ (Alfar Aesar), $\text{Ni}(\text{NO}_3)_2 \cdot 6\text{H}_2\text{O}$ (Alfar Aesar), $\text{Cr}(\text{NO}_3)_3 \cdot 9\text{H}_2\text{O}$ (Aldrich), CrO_3 (Aldrich), CoCl_2 (Aldrich), VCl_3 (Aldrich), RuCl_3 (Aldrich), $\text{FeCl}_3 \cdot 6\text{H}_2\text{O}$ (Aldrich), $\text{YCl}_3 \cdot 6\text{H}_2\text{O}$ (Aldrich), $\text{LaCl}_3 \cdot 7\text{H}_2\text{O}$ (Aldrich), OsCl_3 (Aldrich), PtCl_4 (Aldrich), $\text{Pt}(\text{NH}_3)_4(\text{NO}_3)_2$ (Alfar Aesar), RbClO_4 (MP Biomedicals Inc.).

Synthesis and Characterization of Catalysts

TiO_2 nanoparticles were prepared by standard sol-gel methods. TiO_2 sols were prepared by dropwise addition of 5 mL of an ethanolic TTIP solution, which had been dissolved in 50 mL of absolute ethanol, into 50 mL of distilled water adjusted to pH 1.5 with nitric acid under vigorous stirring at room temperature. After continuously stirring for 24 hours, the resulting transparent solution was evaporated using a rotary evaporator at 45 °C and dried in the oven (70 °C) overnight. The obtained powder was calcined at various temperatures from 200 °C to 700 °C (typically at 400 °C) for 1 hour under air. Metal ion-doped TiO_2 samples (M- TiO_2) were prepared according to the above procedure in the presence of the corresponding metal ion salt precursors to give a doping level from 0.1 to 1.0 atomic-% (at.%). The appropriate amount of metal-ion precursor was added to the distilled water before hydrolysis of TTIP and the remaining procedures were the same as described above. The doped TiO_2 products exhibited a variety of different colors. Doping with Cr^{3+} , Cu^{2+} , and Ni^{2+} produced TiO_2 samples with a green color. Os^{3+} , Pt^{4+}

and Pt^{2+} doping- produced brown products; Ru^{3+} doping yielded a dark brown product; V^{3+} doping produced an orange product; Fe^{3+} doping produced a light orange product; and Co^{2+} doping gave a light yellow TiO_2 product. All the other metal doped samples are white colored.

Crystal structure patterns of the M- TiO_2 powder samples were examined by X-ray diffraction (XRD) using a Philips diffractometer (X'pert Pro) with $\text{Cu-K}\alpha$ radiation. Brunauer-Emmett-Teller (BET) surface area measurement were carried out by using N_2 as the adsorptive gas (Micromeritics Gemini), and the morphology and elemental composition analysis were performed by scanning electron microscopy (SEM, LEO 1550VP) equipped with EDS (Energy Dispersive X-ray Spectroscopy). UV-vis diffuse reflectance spectra (DRS) were obtained on a Shimadzu UV-2101PC spectrophotometer.

Determination of Photocatalytic Activity

The photocatalytic activities of the array of synthesized TiO_2 samples were quantified by measuring the rates of photo-bleaching and degradation of MB, the rates of I^- oxidation, and the rates of degradation of phenol. Synthesized TiO_2 samples were dispersed in distilled water (1 gL^{-1}). This was followed by the addition of an aliquot of the target substrate stock solution to the catalyst suspension to give a specific substrate concentration (i.e., $[\text{MB}]_0 = 10 \text{ }\mu\text{M}$, $[\text{I}^-]_0 = 50 \text{ mM}$, and $[\text{PhOH}]_0 = 50 \text{ }\mu\text{M}$). The reaction suspensions pH were circum-neutral at $t=0$. Before irradiation, the suspension was stirred in the dark for 30 min to obtain a state of sorption equilibrium of the specific substrate on TiO_2 . A high-pressure Hg(Xe) Arc lamp (500 W) was used as the light source. The incident light beam was passed through an IR water filter and a UV cut-off filter giving λ

> 320 nm for UV irradiation or $\lambda > 400$ nm for visible irradiation before being focused onto a cylindrical Pyrex reactor through a quartz window. The reactor was open to ambient laboratory air during photolysis with a few exceptions. Time-sequenced sample aliquots were collected from the reactor during the time-course of illumination for analysis and filtered through a 0.45 μm PTFE syringe filter to remove TiO_2 particles. Multiple photolysis experiments were performed under the identical reaction conditions to determine reproducibility.

The rate constants for the observed degradation of MB during photolysis were determined by measuring the absorbance of sample aliquots at 665 nm with a conventional spectrophotometer. In the case of the photocatalytic oxidation of iodide, triiodide ion (I_3^-), which is the principal product of iodide oxidation in the presence of excess iodide ion, was determined spectrophotometrically by measuring its absorbance at 352 nm. The degradation of phenol in aqueous solution was measured using high performance liquid chromatography (HPLC, HP 1100 series with a C18 column).

Results and Discussion

X-ray Diffraction Analysis of Metal-Ion-Doped TiO_2 (M- TiO_2)

The structure of TiO_2 samples synthesized by standard sol-gel methods appeared to be amorphous thermal annealing; however, post-synthesis treatment at various temperatures ranging from 200 to 700 $^\circ\text{C}$ resulted in higher degree crystallinity primarily as anatase. The increasing calcination temperatures resulted in an increase in the intensity and sharpness of the anatase peaks. This trend is clearly indicative of an improvement in the degree of crystallinity corresponding to the formation of larger particles with fewer

defects. However, above a given temperature XRD peaks corresponding to the rutile phase appear. No diffraction peaks that could be attributed to doping metals were observed. Thus, the crystal structure of TiO_2 indicates a mixture of anatase and rutile for all the synthesized M- TiO_2 samples. These results suggest that at the doping levels we employed or the subsequent thermal treatment did not induce the formation of discrete impurity phases and that the metal ion appears to have been integrated into the basic structure of TiO_2 . However, it is conceivable that metal impurities, which were formed during synthesis, were nanoscopic or possibly dispersed on the surface. We have assumed that some of the metal ion dopants such as Pt^{4+} , Cr^{3+} , and V^{3+} ions are most likely to be substituted at Ti^{4+} sites within TiO_2 because ionic radii of dopants (Pt^{4+} : 0.765 Å, Cr^{3+} : 0.755 Å, and V^{3+} : 0.78 Å) are similar to that of Ti^{4+} (0.745 Å), whereas some other metal dopants such as Co^{2+} , Cu^{2+} and Pt^{2+} ions are possibly located in interstitial positions of the lattice rather than directly in Ti^{4+} sites because of the relatively large size difference between dopant ions (Co^{2+} : 0.89 Å, Cu^{2+} : 0.87 Å and Pt^{2+} : 0.94 Å) and Ti^{4+} . However, Ag^+ , Rb^+ , Y^{3+} and La^{3+} ions seem to be too large to be incorporated in TiO_2 lattice and thus, they are more likely to be found as dispersed metal oxides within the crystal matrix or they are dispersed on the surface of TiO_2 .

The anatase-to-rutile phase transformation (i.e., the A-R phase transformation) of pure TiO_2 normally occurs between 600 and 700 °C.³³⁻³⁶ In our case, pure (undoped) TiO_2 samples that were calcined at 400 °C showed only the anatase phase. Calcination at 700 °C produced with a relatively small fraction of the rutile phase. However, it was observed that, in some cases, metal-ion doping altered the temperature of the A-R phase transformation of TiO_2 . In this regard, the XRD patterns of representative M- TiO_2

samples that were calcined at different temperatures are shown in Figure 2.1. Similar to undoped TiO₂, La-TiO₂ prepared at 400 °C was entirely in the anatase phase. Anatase remained as the dominant phase until a minor rutile component was observed at 700 °C (Figure 2.1a). However, in the case of Pt-TiO₂, a rutile peak at $2\theta = 27.5^\circ$ appeared at 400 °C as shown in Figure 2.1(b). This rutile peak was clearly dominant at 700 °C, while the anatase peak at $2\theta = 25.7^\circ$ disappeared at 700 °C. In comparison, Ru-TiO₂ was almost exclusively pure anatase phase even at 700 °C in Figure 2.1(c), implying Ru ion inhibited A-R phase transformation of TiO₂.

In order to compare the effects of metal-ion doping on the A-R phase transformation, the fraction of rutile, X_R , was calculated from the respective peak intensities using following equation:³⁷

$$X_R (\%) = \{1 - (1 + 1.26I_R/I_A)^{-1}\} \times 100 \quad (2.1)$$

where I_R and I_A are the X-ray intensities of the rutile (101) and anatase (110) peaks, respectively. These relative rutile fractions are listed in Table 2.1 with ionic radii of the dopants. Pt-TiO₂, Cr-, V-, Fe-, Y-, and Rb-TiO₂ also exhibited evidence of a rutile phase after calcinations at 400 °C. Their rutile fractions were estimated to be 15 ~ 30 %, whereas the undoped samples and remaining M-TiO₂ samples were in the pure anatase phase. Pt- and Y-TiO₂, which were calcined at 700 °C, also exhibited high rutile fractions ($X_R = 100\%$ and 62 %, respectively) when compared to undoped TiO₂ ($X_R = 15\%$). Therefore, we conclude that certain dopants Pt, Cr, V, Fe, Y, and Rb) lowered the A-R phase transformation temperature of TiO₂. In the specific case of Ru-TiO₂ calcined at 700 °C, the X_R fraction was estimated to be only 3%, which indicates that Ru increased

the apparent temperature of A-R phase transformation. Similar results have been reported elsewhere.^{1,38-42}

However, some previous studies reported controversial results of doping effect on A-R phase transformation. For example, Ruiz et al.⁴³ reported that Cr-TiO₂ inhibited the A-R phase transformation. However, they observed an additional XRD peaks due to Cr₂O₃ as well as TiO₂. The formation of chromium oxide is most likely due to the high doping level of Cr at 5 ~ 10 at.%. In comparison, no Cr-related peaks were observed at our doping level of Cr (0.3 at.%). Therefore, it is likely that an effect of doping on A-R phase transformation temperature depends on the actual doping concentration. Doping at high Cr ion concentrations, which may result in Cr segregated on TiO₂ surface as opposed to direct substitution in Ti⁴⁺ may impact the A-R phase transformation differently. Some studies also showed that doping with Ce, La, or Y ions also inhibits the A-R phase transformation.^{34,38,44} The inhibiting phenomena of these dopants has been explained in terms of the formation of Ti-O-Ce (or La, Y) bonds at the interface since they could be located primarily on the surface of TiO₂ because of relatively large differences in the ionic radii resulting in inhibited crystal grain growth.^{45,46} A similar inhibition of A-R phase transformation has been pointed out for TiO₂/SiO₂ mixture as well.^{33,36} However, our results indicate that La doping had little impact on the A-R phase transformation, while Y accelerated the transformation. It should be noted that the doping levels of La, Y, and Ce ions in TiO₂ are about 5 ~10 at.% in most studies in contrast to a level of 0.3 at.% in this study. In addition, Ghosh et al.³⁸ showed that peaks due to Y₂Ti₂O₇ or La₄Ti₉O₂₄ were identified in the XRD patterns of Y- or La-doped TiO₂

samples that showed an inhibiting effect on the A-R phase transformation, whereas no Y or La-derived peaks were observed in our XRD results.

In order to investigate the effect of doping level concentration on the A-R phase transformation, the fractions of rutile (X_R) in Pt(II)-TiO₂ with different Pt concentration from 0.1 to 1.0 at.% were determined. As shown in Figure 2.2, X_R fraction increases to approximately 22 % when Pt is doped in the range of 0.1~0.3 at.% and then decreases at higher doping levels in the range of 0.5~1.0 at.%. These results indicate that doping effect of metal ions on the A-R phase transformation is dependent on not only the intrinsic physicochemical properties of doping metal ion but also the concentrations of the dopants. Shannon et al.⁴⁷ also reported that the total impurity content can affect the transformation through the structure stuffing effect and large quantities of impurities may raise the transformation temperatures.

There are only a few concepts or rules to clarify the effects of impurities doped into TiO₂ on the A-R phase transformation. The primary factor that has been invoked in order to explain the doping effect on A-R phase transformation is the creation of oxygen vacancies since the A-R phase transformation involves a contraction or shrinking of the oxygen structure.⁴⁷ It is also believed that impurities can affect the rate of the transformation by modifying the defect structures of TiO₂. Based on this concept, Shannon et al.⁴⁷ suggested that processes that increase oxygen vacancies such as the addition of ions of valence less than four and of small ionic radius which can enter the structure via direct substitution, accelerate the A-R phase transformation (and *vice versa*). They also hypothesized that an increase of oxygen vacancy concentration reduces the strain energy that must be overcome before the rearrangement of Ti-O octahedral occurs.

In addition, Mackenzie et al.⁴⁸ proposed a rank-ordered list of dopants in terms of their effectiveness in accelerating the A-R phase transformation and concluded that monovalent ions are more effective than divalent or trivalent ions since more oxygen vacancies would be created in the doping of monovalent ions compared to divalent or trivalent ions.

According to our results, however, there is no such a correlation observed between valence state of dopant and the fraction of rutile phase of M-TiO₂. For example, the fractions of the rutile phase of Pt(IV)-TiO₂ and Cr(III)-TiO₂ are compared to Pt(II)-TiO₂ and Cr(VI)-TiO₂ in Table 2.1. The doping with Pt(IV) ion also accelerated the A-R phase transformation with the fraction of rutile from 0 % to 26 % and it was similar to rutile fraction of Pt(II)-TiO₂ sample (22 %). With respect to Cr doping, both Cr(VI) and Cr(III) accelerated the A-R phase transformation as well. In addition, the data as shown in Figure 2.3 demonstrates that there are no obvious correlations between X_R in various M-TiO₂ samples as a function of valence state or ionic radius of each metal dopant. Figure 2.3(a) also shows that the doping with monovalent ions was not more effective for A-R phase transformation than divalent or trivalent ions and the fraction of rutile was varied even with the same valence state of dopant ions. Figure 2.3(b) also shows the X_R fraction of the various trivalent ion-doped TiO₂ samples as a function of their ionic radii. It is clear that there is no correlation observed. Therefore, the valence state or ionic radius of dopant metal ion is not a good predictor of the effectiveness of specific dopants on the A-R phase transformation even if oxygen vacancies, which might be induced by metal-ion doping, affect the A-R phase transformation of M-TiO₂ samples.

BET Surface Areas and SEM Characterization

BET surface areas (Table 2.1) were determined using nitrogen adsorption and desorption isotherms. The BET surface area of the unadulterated sol-gel synthesized TiO_2 , which was calcined at $400\text{ }^\circ\text{C}$, was determined to be $104\text{ m}^2\text{ g}^{-1}$. In comparison, the surface area of the commercial product, Degussa P25 TiO_2 , is listed at $50\text{ m}^2\text{ g}^{-1}$ and confirmed by our measurements. The BET surface areas of M- TiO_2 samples were found to be slightly larger than the undoped TiO_2 ($110\sim 130\text{ m}^2\text{ g}^{-1}$ for M- TiO_2 samples). Figure 2.4 shows the change of BET surface areas and rutile fractions of 0.3 at.% Pt(II)- TiO_2 as a function of calcination temperature. The BET surface area of Pt(II)- TiO_2 is $\sim 150\text{ m}^2\text{ g}^{-1}$ without heat treatment and at $200\text{ }^\circ\text{C}$ calcination. Calcination at $400\text{ }^\circ\text{C}$ decreases the observed surface area as the rutile phase appears. At $700\text{ }^\circ\text{C}$, where Pt- TiO_2 is found in the pure rutile phase, the surface area was decreased to $57\text{ m}^2\text{ g}^{-1}$.

The SEM images of Pt- TiO_2 and Cr- TiO_2 particles, which are shown in Figure 2.5, show that the particles are highly aggregated and surfaces are clearly rough. In addition, the characteristic particle sizes become larger at higher calcination temperatures with a corresponding decrease in surface area. Images of other M- TiO_2 samples (which are not shown here) were similar to Pt- TiO_2 (or Cr- TiO_2).

The elemental composition of the various M- TiO_2 samples was estimated by EDS. The EDS spectra of most of M- TiO_2 samples including TiO_2 doped with Pt^{2+} and Ni^{2+} ions (relatively larger ionic radii of metal dopants) showed no apparent signals directly related to metal dopants. These results indicate that these metal ions are well incorporated into TiO_2 lattice (possibly interstitials of TiO_2 in the case of Pt- TiO_2 or Ni- TiO_2) and not located on or near the surface of the particles. On the other hand, the EDS

spectra of the larger ionic radii dopants (M-TiO₂) such as Ag-TiO₂ and Rb-TiO₂ showed the signals of the metal ions, which indicates that these metal-ion dopants (i.e., Ag, Rb, Y, and La) were located near surface region, not incorporated into TiO₂ lattice because of their much larger ionic radii than Ti⁴⁺.

UV-vis Diffuse Reflectance Spectra

The UV-vis diffuse reflectance spectra of the array of metal ion-doped TiO₂ samples are shown in Figure 2.6. The sol-gel synthesized, undoped TiO₂ (TiO₂-SG) and Degussa P25 TiO₂ are characterized by sharp absorption edges at about 400 nm ($E_{bg} \sim 3.1$ eV). However, most of M-TiO₂ samples show extended absorption spectra into visible region in the range of 400 ~ 700 nm. Figure 2.6(a) shows TiO₂ samples doped with Fe, Cu, and Ni ions exhibited relatively small absorption only between 400 and 550 nm, while Co-, Os-, V-, Ru-, or Cr-doped TiO₂ samples showed substantial and broader absorption shoulders up to 700 nm (Figure 2.6b). Figure 2.6(c) illustrates the difference between the absorption spectra of Pt(IV)-TiO₂ and Pt(II)-TiO₂. Pt(II)-TiO₂ shows a much broader absorption over most of the visible region similar to V-TiO₂ (Figure 2.6(b)). However, Pt(IV)-TiO₂ has a smaller absorption peak between 400 and 550 nm.

The extended absorption of the M-TiO₂ samples into the visible region has been explained in terms of the excitation of electrons of dopant ion to TiO₂ conduction band (i.e., a metal to conduction band charge-transfer). For example, the enhanced absorption observed for the M-TiO₂ samples doped with Fe, Cr, V, Co, Ni, and Cu in visible region can be considered to involve excitation of 3d electrons of dopant ion to TiO₂ conduction band according to their respective energy levels.^{2,3,6,7,49-51} However, the absorption

spectra of modified TiO₂ in visible region may originate from defects associated with oxygen vacancies that give rise to colored centers.^{52,53} Kuznetsov and Serpone pointed out the similarities of the spectra in the range of 400~600 nm shown among different types of visible-light-active TiO₂ samples and these similarities were found even in reduced TiO₂ samples.^{52,54,55} They also observed that the absorption spectra were given by the sum of overlapping absorption bands with maxima at 2.81 eV and 2.55 eV, which correlate with oxygen vacancies.^{52,53} In fact, the metal-ion dopants used in this study have different valence states than Ti⁴⁺ and, as a consequence, may induce the generation of oxygen vacancies during synthesis. In addition, similarities of the absorption spectra in the range of 400~600 nm that Kuznetsov et al. observed were also found among several M-TiO₂ samples in this study, even though the absorption intensities were different. Therefore, the generation of new energy levels due to the injection of impurities within the bandgap coupled with the generation of oxygen vacancies by metal-ion doping may contribute to the observed visible-light absorption of the M-TiO₂ samples. Consistent with this hypothesis, we find that there are no visible-light extended absorption spectra for M-TiO₂ with Ag-, Rb-, Y-, and La-TiO₂. As discussed above, the ionic radii of these dopants are too large to substitute with Ti⁴⁺ in the lattice of TiO₂ and are considered to be dispersed on the surface of TiO₂ particles. This interpretation is consistent with the results of the EDS analysis.

Visible-light Photocatalytic Activities of M-TiO₂

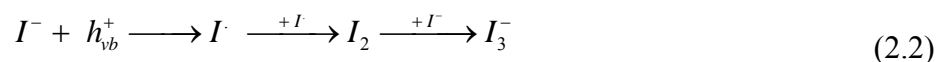
The photo-bleaching and degradation of MB under visible light irradiation follows apparent first-order kinetics. The observed reaction rate constants (k_{MB}) with the various

M-TiO₂, which are prepared at doping level of 0.3 at.% and calcined at 400 °C under both UV and visible-light irradiation, are listed in Table 2.2. Under visible-light irradiation at $\lambda > 400$ nm, k_{MB} for direct photolysis without TiO₂ particles is estimated 0.003 min⁻¹. The observed rate constant was increased slightly to 0.005 min⁻¹ in the presence of undoped TiO₂. This activity may be due to additional light absorption above 400 nm of TiO₂ particles or enhanced direct electron injection from adsorbed MB to the conduction band of TiO₂. However, Pt-, Cr-, V-, Ni-, and Rb-TiO₂ showed significantly enhanced photocatalytic activities under the visible-light irradiation by an order of magnitude ($k_{\text{MB}} > 0.01$ min⁻¹). Among all tested M-TiO₂ samples, Pt-TiO₂ (both Pt(II)-TiO₂ and Pt(IV)-TiO₂) showed the best visible-light photo-activity for MB degradation. Most of other M-TiO₂ samples (i.e., Fe-, Co-, Cu-, Os-, Ag-, and Y-TiO₂) showed slightly increased k_{MB} , while Ru- and La-TiO₂ had negligible effect when compared to undoped TiO₂. None of the M-TiO₂ samples had lower photocatalytic activities when compared to the undoped SG-TiO₂. Under UV irradiation (> 320 nm), Pt-TiO₂ and Rb-TiO₂ had significantly enhanced photocatalytic activities for MB degradation as well. However, Cr- and V-TiO₂, which had comparable k_{MB} values to Pt-TiO₂ under visible-light irradiation, had slightly enhanced photocatalytic activities under UV irradiation.

In some case, the rates of degradation of MB were increased even with several M-TiO₂ samples that did not show extended visible-light absorption. For example, Rb-TiO₂, which has same absorption spectrum as undoped TiO₂, gave a higher k_{MB} value than undoped TiO₂ under visible-light irradiation. In a similar fashion, Ag- and Y-TiO₂ also showed slightly enhanced visible-light photocatalytic activities. Therefore, the enhanced photocatalytic activities of Rb-, Ag-, and Y-TiO₂ for MB degradation were not attributed

to efficient utilization of visible-light with M-TiO₂. It might be due to other effects of dopants located on the surface of TiO₂ such as enhanced transfer of charge carriers generated by visible-light absorbed MB molecules. Therefore, it suggests that MB seems to be inappropriate as model compounds to evaluate photocatalytic activities of new visible-light photocatalysts (i.e., modified TiO₂), and visible-light photocatalytic activity should be evaluated by various reactions. Yan et al.⁵⁶ also reported that the photo-action spectrum for photocatalytic degradation of MB under visible-light irradiation is similar to the photoabsorption spectrum of the dye, which supports their suggestion that the MB molecules directly absorb photons, and thus the photoexcited electrons may be injected into the underlying M-TiO₂. However, some studies only showed extended absorption of modified photocatalysts into visible range and enhanced degradation rates of dyes as compared to unmodified ones and then concluded that their modified photocatalysts have intrinsic visible-light photoactivities.^{3,8,15,16,57,58}

Iodide is oxidized readily by valence-band holes or surface-bound hydroxyl radical in aqueous solution to form tri-iodide (I₃⁻) according to the reaction sequence:



The production of I₃⁻ ions from I⁻ oxidation during photolysis in the presence of Pt-TiO₂ and Cr-TiO₂ is shown in Figure 2.7(a). No I₃⁻ was produced in the absence of TiO₂ particles at λ > 400 nm and undoped TiO₂ showed little photocatalytic activity with respect to the net photo-oxidation of I⁻ to I₃⁻. In contrast, Cr-TiO₂ and Pt(IV)-TiO₂ had significantly enhanced photocatalytic activities with respect to iodide oxidation. Unlike undoped TiO₂, the production of I₃⁻ with Cr-TiO₂ or Pt(IV)-TiO₂ occurred in a relatively fast at initial period of irradiation followed by an approach to a steady-state that may be

due to the reduction of I_3^- to I^- by conduction band electrons (i.e., the rate of the back electron transfer reaction increases as the concentration of I_3^- ions increases and thus a steady-state is achieved).

The comparative photocatalytic activities of the all M-TiO₂ samples ranked in terms of the total amount of I_3^- produced during 15 min of irradiation are given in Table 2.2. Cr-TiO₂ and Pt(IV)-TiO₂ have substantially enhanced visible-light photocatalytic activity for I^- oxidation, while Pt(II)-, V-, and Ni-TiO₂ are slightly enhanced. In contrast, the other M-TiO₂ products had negligible activity during the 15 min reaction time. Unlike the degradation reaction of MB, Ag-, Rb-, Y-, and La-TiO₂ exhibited no enhanced effects on visible-light activities with respect to I^- oxidation.

The oxidation of iodide in suspensions of Pt-, Cr-, V-, and Ni-TiO₂, which showed enhanced visible-light photocatalytic activities, were also investigated under UV irradiation at $\lambda > 320$ nm. In the case of UV light illumination, Pt-TiO₂ had a higher photoactivity than undoped TiO₂. However, the other M-TiO₂ materials showed almost same photocatalytic activities as undoped TiO₂. Pt(II)-TiO₂ had comparable photocatalytic activities to Pt(IV)-TiO₂ under UV irradiation, whereas it had lower photoactivity than Pt(IV)-TiO₂ under visible-light irradiation.

The photocatalytic degradation of phenol vs. time in suspensions of Pt-TiO₂ and Cr-TiO₂ under visible-light irradiation is shown in Figure 2.7(b). Pt(IV)-TiO₂ was also the most effective photocatalyst for phenol degradation. Pt(II)-TiO₂ and Cr-TiO₂ also showed significantly enhanced visible-light photocatalytic activity, while V-TiO₂ had a moderately enhanced photoactivity. The results in terms of phenol degradation were similar to those observed for I^- oxidation. However, the other M-TiO₂ materials did not

show any improvement in photocatalytic activities for phenol degradation under visible-light irradiation as shown in Table 2.2.

From our kinetics observations, we can conclude that the visible-light photocatalytic activities of various M-TiO₂ materials are not directly correlated with their corresponding UV-vis absorption spectra of M-TiO₂. For example, Ru- and Os-TiO₂ did not have significant visible-light photocatalytic activities, even though they had extended absorption bands above 420 nm. V-TiO₂, which has larger visible absorption than Cr- and Pt-TiO₂, was found to be less active under visible light illumination. The efficient absorption of visible-light does not appear to be a decisive factor that determines the visible-light photocatalytic activity of M-TiO₂, although visible-light absorption is clearly necessary to initiate photo-reactions. Moreover, visible-light photocatalytic activity of M-TiO₂ material also appears to be substrate-dependent. For MB degradation, most of M-TiO₂ samples were found to have enhanced photocatalytic activities, although Pt-, Cr-, V-, Ni-, and Rb-TiO₂ were clearly the most efficient. The photo-oxidation rate of I⁻ under visible-light irradiation was increased with Pt-, Cr-, V-, Ni-, and Fe-TiO₂ samples. However, only Pt-TiO₂ and Cr-TiO₂ showed significantly enhanced activities for the degradation of phenol. Therefore, it seems to be difficult to correlate visible-light photocatalytic activities with certain obvious physicochemical properties such as color, surface area, and absorption of M-TiO₂ materials as a function of the variation in M. However, it is interesting to note that visible-light photocatalytic activity of M-TiO₂ materials was influenced by the fraction of rutile in M-TiO₂. Pt-TiO₂ and Cr-TiO₂, which showed the most enhanced visible-light photocatalytic activities for all tested reactions, have higher fractions of rutile in TiO₂ as shown in Table 2.1. On the other hand, Ru-TiO₂

and Os-TiO₂, having pure anatase structure, did not show significantly enhanced visible-light photocatalytic activities for all reactions, although they exhibited relatively large absorption in visible region of the spectrum. In cases of Rb-TiO₂ and Y-TiO₂, even though they had relatively high rutile contents, no enhancement in visible-light photoactivity was observed, since they had no measurable absorption in the visible region.

In order to investigate the effect of the fraction of rutile on visible-light photocatalytic activity, the photo-bleaching and degradation rate constants of MB, k_{MB} , under visible-light irradiation were measured as a function of the fractional content of rutile, X_R , in Pt(II)-TiO₂ calcined at 400 °C with different doping levels. As shown in Figure 2.8, k_{MB} is increased with an increasing fractional content of rutile in Pt-TiO₂. This result suggests clearly that the fractional content of rutile in TiO₂ plays an important role in photocatalytic activity in our experiments.

TiO₂ particles in rutile phase are generally considered to be much less photochemically active than their anatase phase counterparts.⁵⁹⁻⁶¹ However, there are a number of specific chemical reactions for which higher photoactivity has been reported with rutile as the photocatalyst.^{62,63} For example, Kim et al.⁶³ reported the Ni-TiO₂ in the rutile phase had a much higher photocatalytic activity than the anatase form of Ni-TiO₂ for the decomposition of 4-chlorophenol under both UV and visible light irradiation, whereas they found the anatase phase of undoped TiO₂ have higher photocatalytic activity than undoped rutile. Furthermore, Torimoto and Ohtani⁵⁹ established that the photoactive crystalline phase of anatase/rutile mixed TiO₂ powder is dependent even on the kind of photocatalytic reaction. They observed that the photoreactivities of TiO₂ in

anatase/rutile mixed phase for H₂ production were between pure anatase and pure rutile and shifted toward that of pure rutile with increase of rutile fraction; whereas the photoreactivities of mixed TiO₂ for Ag deposition and acetic acid decomposition were similar to that of pure rutile and pure anatase phases, respectively, and not dependent on the rutile fraction. In addition, it has been reported that TiO₂ in anatase/rutile mixed phases have higher activity than the pure anatase phase alone under UV irradiation.^{60,64,65} Another example from our study shows that the visible-light photocatalytic activity of Pt(II)-TiO₂ with respect to I⁻ oxidation is strongly influenced by the calcination temperature. The photocatalytic activity of Pt-TiO₂ gave a maximum at 400 °C where a mixed rutile/anatase structure of Pt-TiO₂ predominates. The pure anatase end member of Pt-TiO₂ at 200 °C and pure rutile end member of Pt-TiO₂ at 700 °C clearly were less photoactive than mixed-phase structural form of Pt-TiO₂ at 400 °C.

Higher photocatalytic activities of Pt-TiO₂ or Cr-TiO₂ having a significant fraction of the rutile phase due to calcinations at 400 °C may be due to a larger number of oxygen vacancies⁶⁶⁻⁶⁸. For example, Li et al.⁶⁸ proposed that the formation of sub-energy defect level in Ce-TiO₂ may be one of the critical reasons to reduce the recombination of electron-hole pairs and to enhance photocatalytic activity. Ihara et al. also reported that the oxygen deficient TiO₂ induced by RF H₂ plasma treatment (without doping) absorbed visible light and showed visible light photocatalytic activity.^{69,70} In a similar fashion, the formation of oxygen vacancies in Pt-TiO₂ or Cr-TiO₂, which results in a lowering of the temperature of the A-R phase transformation leading to a rutile structure at 400 °C, appears to lead to an enhancement of the photocatalytic activities of M-TiO₂ under visible-light irradiation.

Our group previously investigated metal-ion doping on photocatalytic activities of TiO₂ under UV light irradiation in terms of the transient charge-carrier recombination dynamics.^{19,42,71,72} Choi et al.¹⁹ used laser flash photolysis measurements to show that the lifetimes of the blue electron in the Fe-, V-, Mo-, and Ru-doped TiO₂ were increased to ~50 ms, whereas undoped Q-sized TiO₂ had a shorter lifetime of < 200 μs. Hoffmann and co-workers found a good correlation between experimental quantum yields for oxidation or reduction and the measured absorption signals of the charge carriers that survived from recombination over nano- to microsecond time domain (i.e., an increase in concentration of the long-lived charge carriers is expected to result in higher photoreactivity). In addition, Martin et al.^{42,71,72} used time-resolved microwave conductivity (TRMC) measurements of various TiO₂ samples including V-TiO₂ and Fe-TiO₂. The charge-carrier recombination lifetime and the interfacial electron-transfer rate constants were estimated from the decays of TRMC signals and also found to correlate well with measured quantum efficiencies. Furthermore, in the case of V-doped TiO₂, the vanadium doping was shown to influence photoreactivity varied in samples prepared at different sintering temperatures.⁴² For examples, V(IV) is found to reduce the photoreactivity of TiO₂ by promoting charge-carrier recombination via electron trapping at $>VO_2^+$ present in V-TiO₂ (25 °C) or via hole trapping at V(IV) impurities in surficial V₂O₅ islands on V-TiO₂ (200 or 400 °C); whereas in case of V-TiO₂ prepared at 600 or 800 °C, substitutional V(IV) in the lattice of TiO₂ appears to act as a charge-carrier recombination center that resulted in reduced photoreactivity. The above observations emphasize that metal-ion dopants influence the photoreactivity of TiO₂ by altering the charge-carrier recombination and interfacial charge-transfer rate constants. In

conclusion, we believe that these effects are also important for the M-TiO₂ materials prepared as part of this study as well.

Conclusions

In conclusion, we have synthesized an array of metal-doped titanium dioxide materials, M-TiO₂, in order to evaluate their visible-light photocatalytic activities. Pt-, Cr-, V-, Fe-, Rb-, Y-TiO₂ lowered the temperature of the anatase-to-rutile phase transformation whereas Ru-TiO₂ increased the temperature of A-R phase transformation. The fraction of rutile in M-TiO₂ is observed to be dependent on the doping level. However, there appears to be no correlation between the effectiveness of an individual dopant on the A-R phase transformation and its valence state or ionic radius, as previously suggested.^{47,48} The majority of M-TiO₂ materials prepared herein gave absorption spectra that were extended into visible beyond 400 nm. Ag-, Rb-, Y-, and La-TiO₂ did not change the original absorption spectrum of pristine SG-TiO₂. As verified by EDS analysis, the latter group of ions were most likely not incorporated into the lattice of TiO₂ and most likely concentrated in near surface region because of their relatively large ionic radii. The photocatalytic activities of M-TiO₂ were evaluated for MB degradation, I⁻ oxidation, and phenol degradation under visible-light irradiation at $\lambda > 400$ nm. Pt-TiO₂ and Cr-TiO₂, which were prepared at a 0.3 at% doping level and annealed at 400 °C, had a relatively high fraction of rutile and showed significantly enhanced photocatalytic activity compared to SG-TiO₂ for all test reactions under visible-light irradiation. These results indicate that the presence of the rutile structure in the doped TiO₂ may affect photocatalytic activities of M-TiO₂. Pt-TiO₂ substantially improved the observed

photocatalytic activity under UV irradiation at $\lambda > 320$ nm as well. On the other hand, V-, Rb-, Ni-, and Fe-TiO₂ showed visible-light photocatalytic activities only for one or two of the three test reactions.

Acknowledgements

We gratefully acknowledge the generous support for this research that has been provided by the Northrop-Grumman Corporation. In particular, we would like to give special credit to Dr. Ronald Pirich for his enthusiastic encouragement and intellectual support for our joint projects over the years.

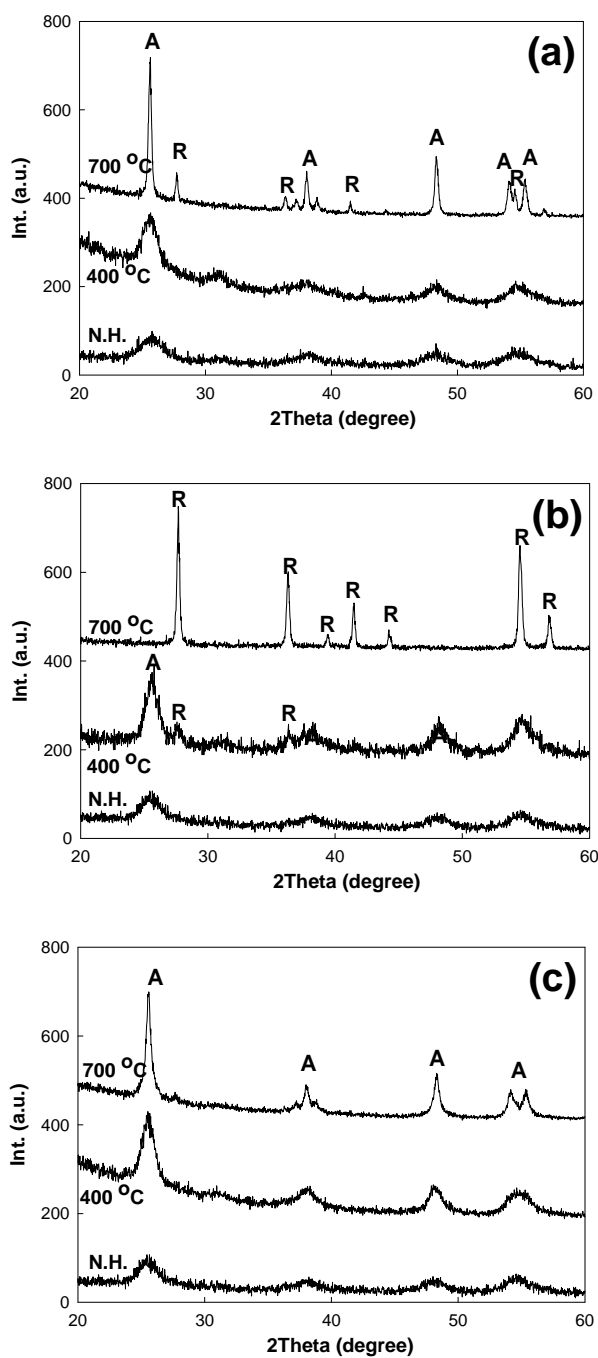


Figure 2.1. X-ray diffraction pattern measured for (a) 0.3 at.% La-TiO₂, (b) 0.3 at.% Pt-TiO₂, (c) 0.3 at.% Ru-TiO₂ with various calcination temperatures (at 700 °C, 400 °C, and no heat treatment)

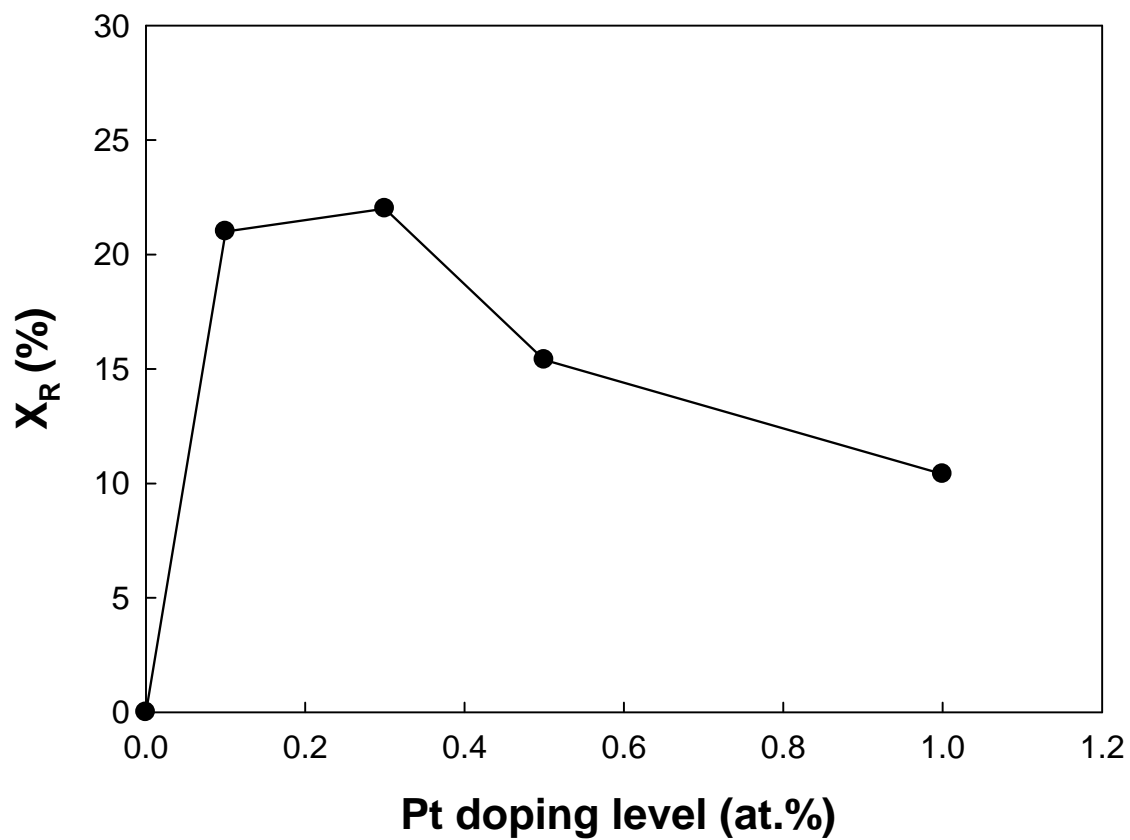


Figure 2.2. The fraction of rutile (%) as a function of doping level of Pt(II) in TiO_2 (at.%). Samples have been prepared by sol-gel method and calcined at 400 °C for 1 hour.

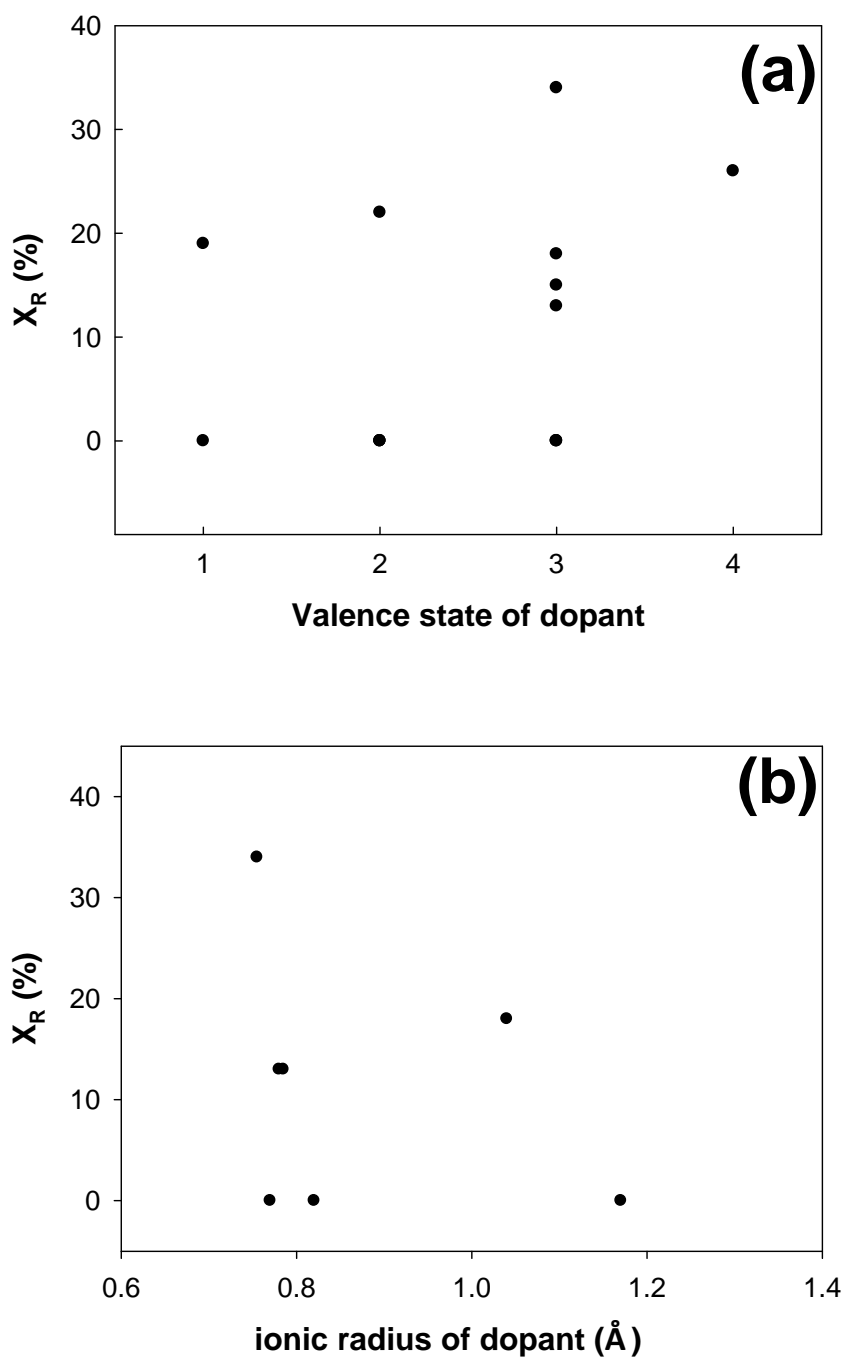


Figure 2.3. The fraction of rutile phase (%) in $M\text{-TiO}_2$ as a function of (a) valence state of dopant and (b) ionic radius of trivalent ion dopants

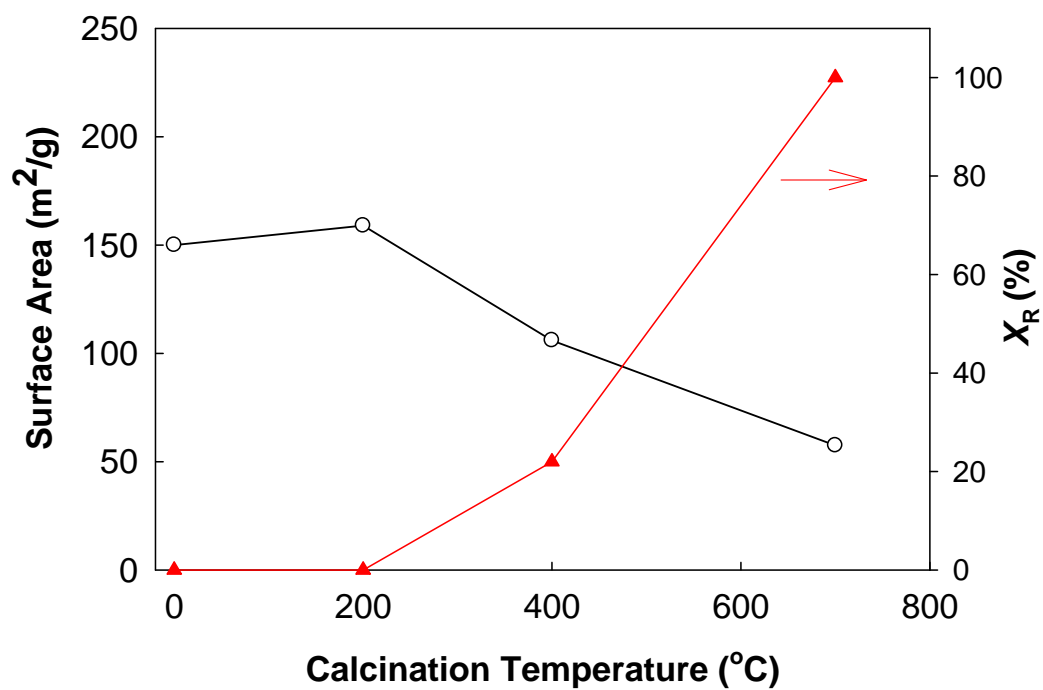


Figure 2.4. BET surface area and the fraction of rutile (X_R) of 0.3 at.% Pt-TiO₂ as function of calcination temperature.

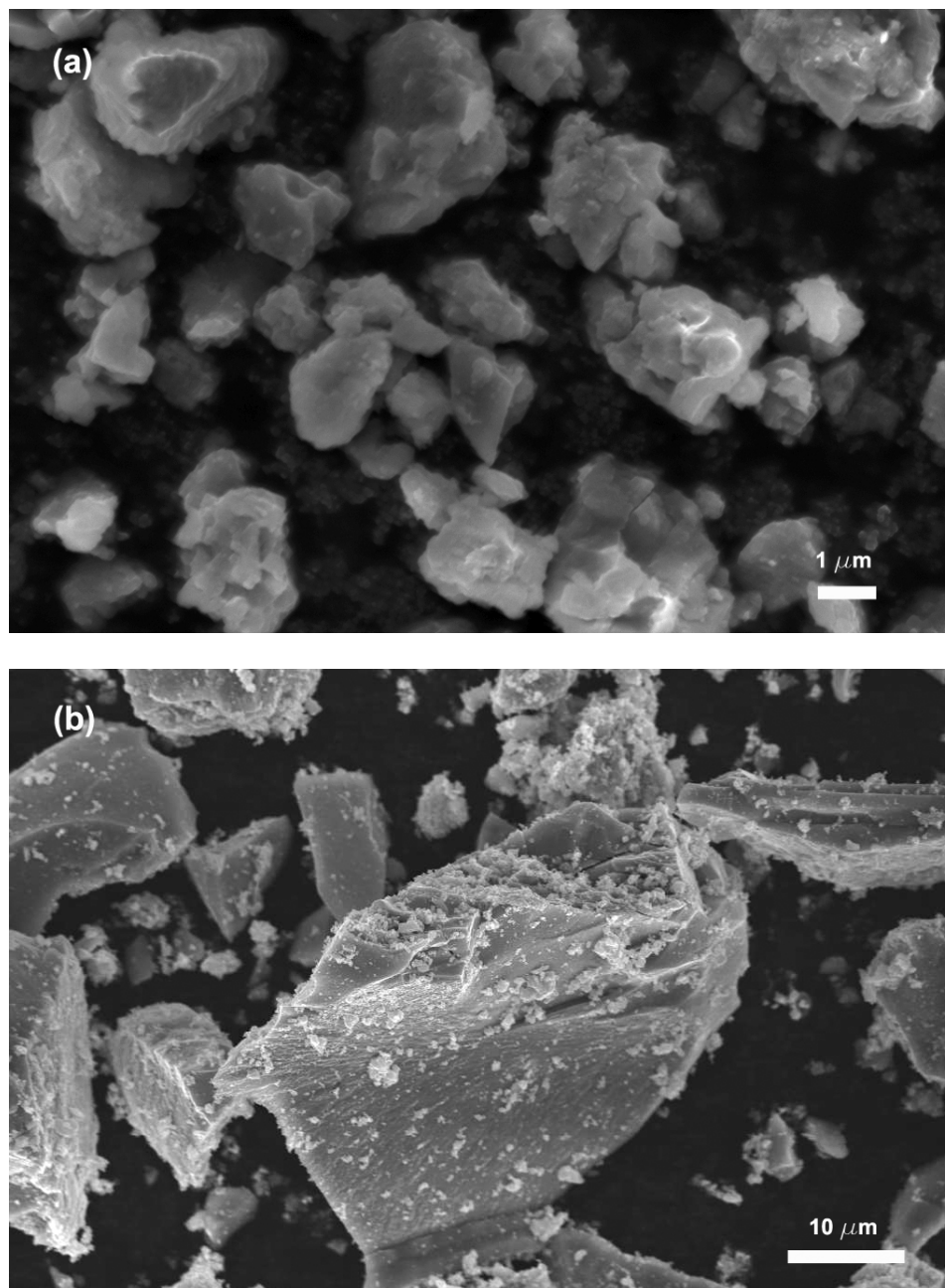


Figure 2.5. SEM images of (a) 0.3 at.% Pt-TiO₂ and (b) 0.3 at.% Cr-TiO₂ synthesized by sol-gel method with 400 °C calcination.

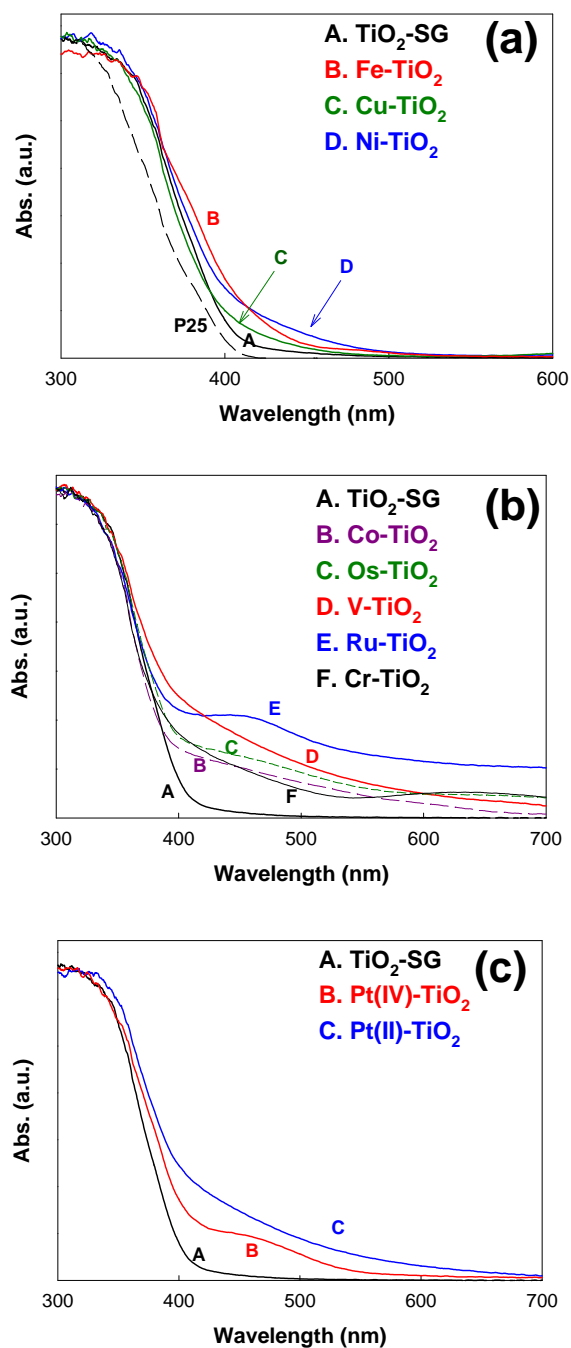


Figure 2.6. UV-vis diffuse reflectance spectra (DRS) for various M-TiO₂ samples (0.3 at.% doping). Absorption spectra for Ag-, Rb-, Y-, and La- TiO₂ samples, which are not shown here, are identical with that of undoped TiO₂.

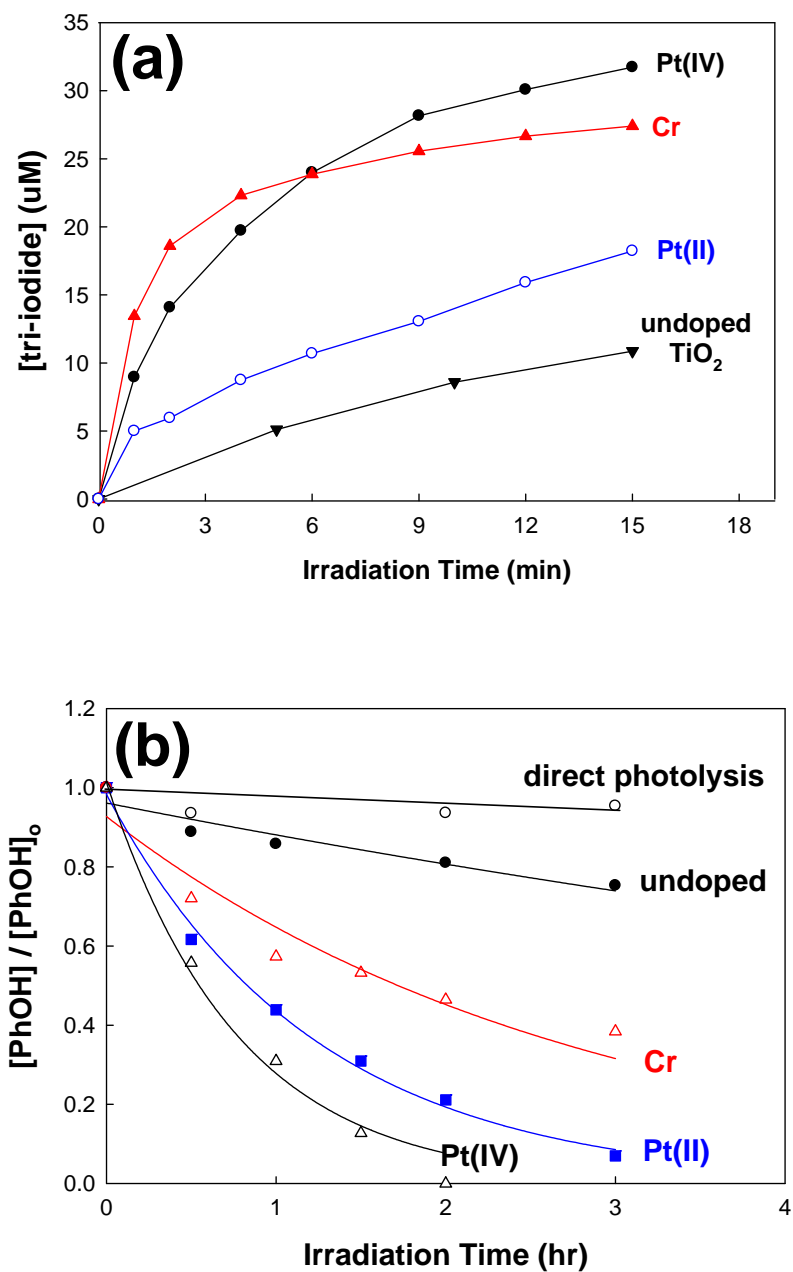


Figure 2.7. Visible-light photocatalytic activities of 0.3 at.% Pt-TiO₂ and 0.3 at.% Cr-TiO₂: (a) The production of tri-iodide by iodide oxidation with $[I^-]_0 = 50$ mM, (b) the degradation of phenol with $[\text{phenol}]_0 = 50$ μM . (total volume = 30 mL, 1 g/L suspension, 500 W, $\lambda > 400$ nm)

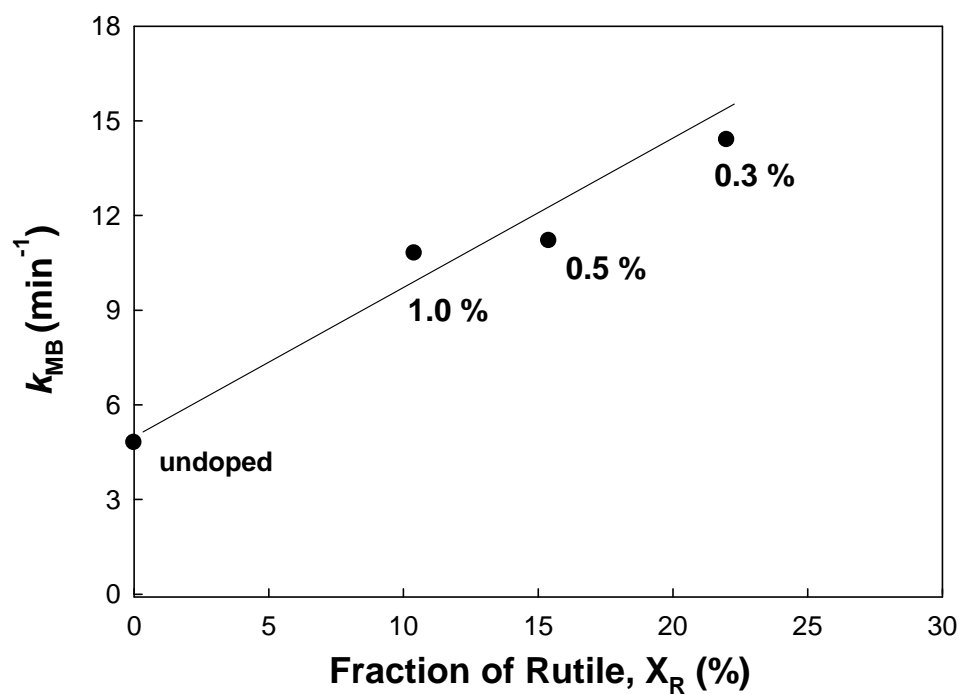


Figure 2.8. Correlation between photocatalytic activities for MB degradation (the degradation rate constant, k_{MB}) at > 400 nm irradiation and the fractions of rutile (X_R) in Pt-TiO₂ prepared at 400 °C with different doping level

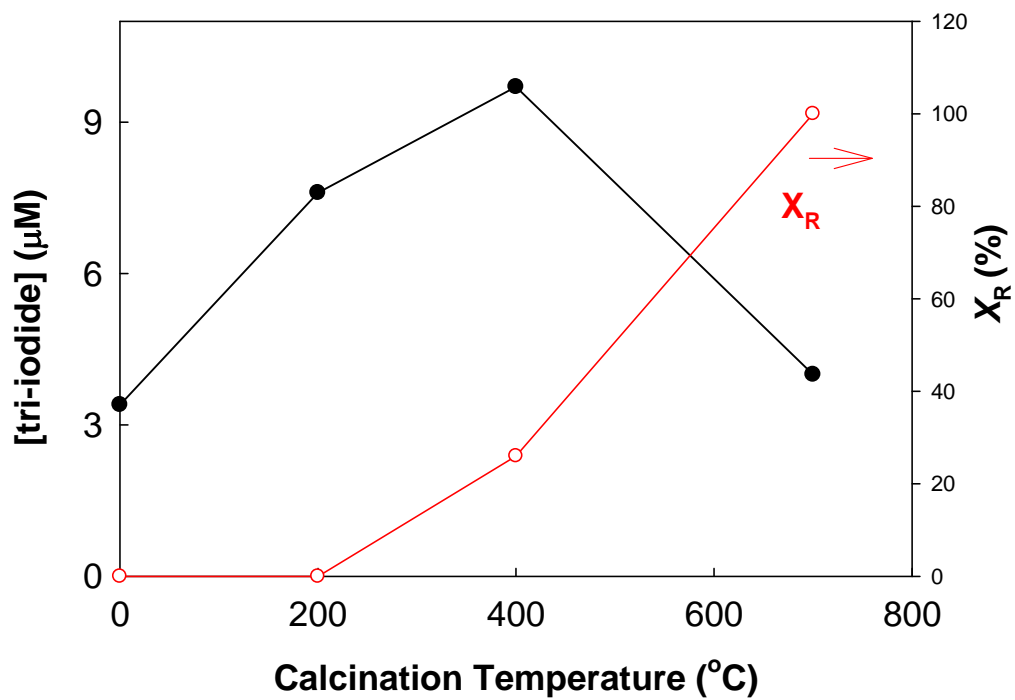


Figure 2.9. Photocatalytic activities for I⁻ oxidation in terms of the amount of I₃⁻ (μM) produced after 6 min at > 400 nm irradiation and the fractions of rutile (X_R) of 0.3 at.% Pt-TiO₂ as function of calcination temperature

TABLE 2.1: Ionic radii of dopants, rutile content by XRD, surface area, and color of various metal ion-doped TiO₂ nanoparticles (at 0.3 at.% doping)

Dopant	Ion size ^a (Å)	Rutile (%)	Surface Area (m ² g ⁻¹)	Color ^e
@ 400 °C calcination				
Undoped TiO ₂	0.745	0	104	White
Pt (II)	0.940	22	111	Light brown
Pt (IV)	0.765	26	106	Light brown
Cr (III)	0.755	34	115	Green
Cr (VI)	0.580	29	125	Green
V (III)	0.780	13	132	Orange
Ru (III)	0.820	0	112	Dark brown
Ni (II)	0.830	0	112	Green
Fe (III)	0.785 ^b	13	113	Light orange
Co (II)	0.885 ^b	0	102	Light yellow
Cu (II)	0.870	0	110	Light green
Os (III)	0.770 ^c	0	117	Light brown
Ag (I)	1.290	0	117	White
Rb (I)	1.660	19	108	White
Y (III)	1.040	18	121	White
La (III)	1.170	0	132	White
@ 700 °C calcination				
Undoped TiO ₂		15		
Pt (II)		100		
Y (III)		62		
La (III)		18		
Ru (III)		3		

^a from literature: Shannon, R. D. *Acta Crystallographica Section A* **1976**, 32, 751.

^b values for high spin in literature (a)

^c value for Os (IV), no available value for Os (III) in literature (a)

^d from literature: Ryu, J. *Environ. Sci. Technol.* **2008**, 42, 294.

^e with samples before heat treatment

TABLE 2.2: Visible-light photocatalytic activities of various M-TiO₂ samples for the degradation of methylene blue (MB), the oxidation of iodide (I⁻), and the degradation of phenol (PhOH)

Dopant	k_{MB} (min⁻¹)		[I₃⁻]_{prod.15min} (μM)		k_{PhOH} (hr⁻¹)
	Vis	UV	Vis	UV	Vis
<i>Direct Photolysis</i>	0.003	0.011	0	0	0
Undoped TiO ₂	0.005	0.014	10	24	0.09
Pt (II)	0.014	0.053	19	40	0.80
Pt (IV)	0.013	0.057	32	42	1.29
Cr (III)	0.013	0.016	27	25	0.36
V (III)	0.012	0.015	16	21	0.13
Ni (II)	0.011	0.010	15	27	0.09
Ru (III)	0.005	0.007	8		0.07
Fe (III)	0.007	0.015	12		0.10
Cu (II)	0.009	0.016	8		0.08
Co (II)	0.009	0.015	12		0.11
Os (III)	0.009	0.013	12		0.09
Ag (I)	0.008	0.016	12		0.07
Rb (I)	0.011	0.033	12		0.07
Y (III)	0.007	0.018	9		0.08
La (III)	0.005	0.016	10		0.10

References

- (1) Zhang, X. W.; Lei, L. C. *Mater. Lett.* **2008**, *62*, 895.
- (2) Nahar, S.; Hasegawa, K.; Kagaya, S. *Chemosphere* **2006**, *65*, 1976.
- (3) Zhu, J. F.; Chen, F.; Zhang, J. L.; Chen, H. J.; Anpo, M. *J. Photochem. Photobiol. A-Chem.* **2006**, *180*, 196.
- (4) Niishiro, R.; Kato, H.; Kudo, A. *Phys. Chem. Chem. Phys.* **2005**, *7*, 2241.
- (5) Kim, D. H.; Lee, K. S.; Kim, Y. S.; Chung, Y. C.; Kim, S. J. *J. Am. Ceram. Soc.* **2006**, *89*, 515.
- (6) Iketani, K.; Sun, R. D.; Toki, M.; Hirota, K.; Yamaguchi, O. *Mater. Sci. Eng., B* **2004**, *108*, 187.
- (7) Klosek, S.; Raftery, D. *J. Phys. Chem. B* **2001**, *105*, 2815.
- (8) Wu, J. C. S.; Chen, C. H. *J. Photochem. Photobiol., A* **2004**, *163*, 509.
- (9) Borgarello, E.; Kiwi, J.; Gratzel, M.; Pelizzetti, E.; Visca, M. *J. Am. Chem. Soc.* **1982**, *104*, 2996.
- (10) Anpo, M.; Ichihashi, Y.; Takeuchi, M.; Yamashita, H. *Sci. Technol. Catal.* **1999**, *121*, 305.
- (11) Pan, C. C.; Wu, J. C. S. *Mater. Chem. Phys.* **2006**, *100*, 102.
- (12) Asahi, R.; Morikawa, T.; Ohwaki, T.; Aoki, K.; Taga, Y. *Science* **2001**, *293*, 269.
- (13) Gole, J. L.; Stout, J. D.; Burda, C.; Lou, Y. B.; Chen, X. B. *J. Phys. Chem. B* **2004**, *108*, 1230.
- (14) Mrowetz, M.; Balcerski, W.; Colussi, A. J.; Hoffman, M. R. *J. Phys. Chem. B* **2004**, *108*, 17269.
- (15) Umebayashi, T.; Yamaki, T.; Tanaka, S.; Asai, K. *Chem. Lett.* **2003**, *32*, 330.
- (16) Wang, Y.; Meng, Y. L.; Ding, H. M.; Shan, Y. K.; Zhao, X.; Tang, X. Z. *J. Phys.*

Chem. C **2008**, *112*, 6620.

(17) Yang, X.; Cao, C.; Hohn, K.; Erickson, L.; Maghirang, R.; Hamal, D.; Klabunde, K. *J. Catal.* **2007**, *252*, 296.

(18) Tachikawa, T.; Tojo, S.; Kawai, K.; Endo, M.; Fujitsuka, M.; Ohno, T.; Nishijima, K.; Miyamoto, Z.; Majima, T. *J. Phys. Chem. B* **2004**, *108*, 19299.

(19) Choi, W. Y.; Termin, A.; Hoffmann, M. R. *J. Phys. Chem.* **1994**, *98*, 13669.

(20) Karakitsou, K. E.; Verykios, X. E. *J. Phys. Chem.* **1993**, *97*, 1184.

(21) Soria, J.; Conesa, J. C.; Augugliaro, V.; Palmisano, L.; Schiavello, M.; Sclafani, A. *J. Phys. Chem.* **1991**, *95*, 274.

(22) Chen, J. H.; Yao, M. S.; Wang, X. L. *J. Nano. Res.* **2008**, *10*, 163.

(23) Di Paola, A.; Garcia-Lopez, E.; Ikeda, S.; Marci, G.; Ohtani, B.; Palmisano, L. *Catal. Today* **2002**, *75*, 87.

(24) Kim, S.; Hwang, S. J.; Choi, W. Y. *J. Phys. Chem. B* **2005**, *109*, 24260.

(25) Ohno, T.; Tanigawa, F.; Fujihara, K.; Izumi, S.; Matsumura, M. *J. Photochem. Photobiol. A-Chem.* **1999**, *127*, 107.

(26) Amadelli, R.; Samiolo, L.; Maldotti, A.; Molinari, A.; Valigi, M.; Gazzoli, D. *Int. J. Photoenergy* **2008**,

(27) Iwasaki, M.; Hara, M.; Kawada, H.; Tada, H.; Ito, S. *J. Colloid Interface Sci.* **2000**, *224*, 202.

(28) Anpo, M. *Pure Appl. Chem.* **2000**, *72*, 1787.

(29) Amadelli, R.; Samiolo, L.; Maldotti, A.; Molinari, A.; Valigi, M.; Gazzoli, D. *Int. J. Photoenergy* **2008**, *9*.

(30) Lettmann, C.; Hinrichs, H.; Maier, W. F. *Angew. Chem., Int. Ed.* **2001**, *40*, 3160.

- (31) Woodhouse, M.; Parkinson, B. A. *Chem. Soc. Rev.* **2009**, 38, 197.
- (32) Sohn, J. M.; Oh, K. S.; Woo, S. I. *Korean J. Chem. Eng.* **2004**, 21, 123.
- (33) Ding, Z.; Lu, G. Q.; Greenfield, P. F. *J. Phys. Chem. B* **2000**, 104, 4815.
- (34) Jing, L. Q.; Sun, X. J.; Xin, B. F.; Wang, B. Q.; Cai, W. M.; Fu, H. G. *J. Solid State Chem.* **2004**, 177, 3375.
- (35) Pillai, S. C.; Periyat, P.; George, R.; McCormack, D. E.; Seery, M. K.; Hayden, H.; Colreavy, J.; Corr, D.; Hinder, S. J. *J. Phys. Chem. C* **2007**, 111, 1605.
- (36) Anderson, C.; Bard, A. J. *J. Phys. Chem. B* **1997**, 101, 2611.
- (37) Spurr, R. A.; Myers, H. *Anal. Chem.* **1957**, 29, 760.
- (38) Ghosh, S. K.; Vasudevan, A. K.; Rao, P. P.; Warriar, K. G. K. *Br. Ceram. Trans.* **2001**, 100, 151.
- (39) Borkar, S. A.; Dharwadkar, S. R. *J. Therm. Anal. Calorim.* **2004**, 78, 761.
- (40) Matteucci, F.; Cruciani, G.; Dondi, M.; Raimondo, M. *Ceram. Int.* **2006**, 32, 385.
- (41) Iida, Y.; Ozaki, S. *J. Am. Ceram. Soc.* **1961**, 44, 120.
- (42) Martin, S. T.; Morrison, C. L.; Hoffmann, M. R. *J. Phys. Chem.* **1994**, 98, 13695.
- (43) Ruiz, A. M.; Sakai, G.; Cornet, A.; Shimanoe, K.; Morante, J. R.; Yamazoe, N. *Sensors and Actuators B-Chemical* **2003**, 93, 509.
- (44) Sibin, C. P.; Kumar, S. R.; Mukundan, P.; Warriar, K. G. K. *Chem. Mater.* **2002**, 14, 2876.
- (45) Ruiz, A. M.; Cornet, A.; Morante, J. R. *Sens. Actuators, B* **2004**, 100, 256.
- (46) Ogata, S.; Iyetomi, H.; Tsuruta, K.; Shimojo, F.; Nakano, A.; Kalia, R. K.; Vashishta, P. *J. Appl. Phys.* **2000**, 88, 6011.
- (47) Shannon, R. D.; Pask, J. A. *J. Am. Ceram. Soc.* **1965**, 48, 391.

- (48) Mackenzie, K. J. D. *Trans. J. British Ceram. Soc.* **1975**, *74*, 29.
- (49) Umebayashi, T.; Yamaki, T.; Itoh, H.; Asai, K. *J. Phys. Chem. Solids* **2002**, *63*, 1909.
- (50) Zhao, Z. Y.; Liu, Q. J.; Zhang, J.; Zhu, Z. Q. *Acta Physica Sinica* **2007**, *56*, 6592.
- (51) Kudo, A.; Niishiro, R.; Iwase, A.; Kato, H. *Chem. Phys.* **2007**, *339*, 104.
- (52) Kuznetsov, V. N.; Serpone, N. *J. Phys. Chem. B* **2006**, *110*, 25203.
- (53) Serpone, N. *J. Phys. Chem. B* **2006**, *110*, 24287.
- (54) Lisachenko, A. A.; Kuznetsov, V. N.; Zakharov, M. N.; Mikhailov, R. V. *Kinet. Catal.* **2004**, *45*, 189.
- (55) Kuznetsov, V. N.; Krutitskaya, T. K. *Kinet. Catal.* **1996**, *37*, 446.
- (56) Yan, X. L.; Ohno, T.; Nishijima, K.; Abe, R.; Ohtani, B. *Chem. Phys. Lett.* **2006**, *429*, 606.
- (57) Ohno, T.; Tsubota, T.; Nishijima, K.; Miyamoto, Z. *Chem. Lett.* **2004**, *33*, 750.
- (58) Bettinelli, M.; Dallacasa, V.; Falcomer, D.; Fornasiero, P.; Gombac, V.; Montini, T.; Romano, L.; Speghini, A. *J. Hazard. Mater.* **2007**, *146*, 529.
- (59) Torimoto, T.; Nakamura, N.; Ikeda, S.; Ohtani, B. *Phys. Chem. Chem. Phys.* **2002**, *4*, 5910.
- (60) Zhang, Q. H.; Gao, L.; Guo, J. K. *Appl. Catal., B* **2000**, *26*, 207.
- (61) Lucarelli, L.; Nadtochenko, V.; Kiwi, J. *Langmuir* **2000**, *16*, 1102.
- (62) Addamo, M.; Bellardita, M.; Di Paola, A.; Palmisano, L. *Chem. Commun.* **2006**, 4943.
- (63) Kim, D. H.; Choi, D. K.; Kim, S. J.; Lee, K. S. *Catal. Commun.* **2008**, *9*, 654.
- (64) Bakardjieva, S.; Subrt, J.; Stengl, V.; Dianez, M. J.; Sayagues, M. J. *Appl. Catal.,*

B **2005**, 58, 193.

(65) Jung, K. Y.; Park, S. B. *J. Photochem. Photobiol. A-Chem.* **1999**, 127, 117.

(66) Yang, J.; Bai, H. Z.; Jiang, Q.; Lian, H. S. *Thin Solid Films* **2008**, 516, 1736.

(67) Kim, H. Y.; Lee, H. M.; Pala, R. G. S.; Shapovalov, V.; Metiu, H. *J. Phys. Chem. C* **2008**, 112, 12398.

(68) Li, F. B.; Li, X. Z.; Hou, M. F.; Cheah, K. W.; Choy, W. C. H. *Appl. Catal., A* **2005**, 285, 181.

(69) Ihara, T.; Miyoshi, M.; Ando, M.; Sugihara, S.; Iriyama, Y. *J. Mater. Sci.* **2001**, 36, 4201.

(70) Ihara, T.; Miyoshi, M.; Iriyama, Y.; Matsumoto, O.; Sugihara, S. *Appl. Catal., B* **2003**, 42, 403.

(71) Martin, S. T.; Herrmann, H.; Choi, W. Y.; Hoffmann, M. R. *Journal of the Chemical Society-Faraday Transactions* **1994**, 90, 3315.

(72) Martin, S. T.; Herrmann, H.; Hoffmann, M. R. *Journal of the Chemical Society-Faraday Transactions* **1994**, 90, 3323.